Scientific paper

Enhanced Adsorption of Methylene Blue by Chemically Modified Materials Derived from *Phragmites australis* Stems

Bui Thi Minh Nguyet,[1] Nguyen Huu Nghi,[1] Nguyen Anh Tien,[2] Dinh Quang Khieu,[3] Ha Danh Duc[1] and Nguyen Van Hung[1,*]

[1] *Dong Thap University, Cao Lanh City, 81000, Vietnam*

[2] *Ho Chi Minh City University of Education, Ho Chi Minh City, 700000, Vietnam*

[3] *University of Sciences, Hue University, 530000, Vietnam*

* *Corresponding author: E-mail: nguyenvanhung@dthu.edu.vn*

Received: 05-05-2022

Abstract

In this study, the biomass of *Phragmites australis* was chemically modified using NaOH and subsequently citric acid to produce an effective adsorbent named SA-RPB. The absorbent was characterized using XRD, SEM, BET, and FT-IR methods. The study's findings indicated that the adsorbent existed mainly as cellulose crystals, contained micropores with an average diameter of 15.97 nm, and had a large number of hydroxyl and carboxyl groups on the surface. The adsorption process of SA-RPB was evaluated through the adsorption of methylene blue (MB) dye in aqueous solution. Adsorption kinetics showed that the pseudo-second-order model well described the adsorption process. The adsorption isotherm process satisfactorily fitted with the Langmuir model with the maximum adsorption capacity of 191.49 mg/g at 303 K. These findings show that MB may be efficiently removed from aqueous solutions using the adsorbent made from the raw biomass of *Phragmites australis* treated with NaOH and then citric acid.

Keywords: Adsorbent; *Phragmites australis*; Methylene blue; Kinetics; Adsorption mechanism

1. Introduction

Dye has been extensively used in various industries such as textile, leather, cosmetics, tanning, paper, food technology, hair coloring, pulp mill, pharmaceuticals, and plastics.[1] Wastewater discharged from these industries has reportedly caused severe environmental pollution[2] and health problems. Specifically, methylene blue (MB), widely used for coloring cotton, wood, and silk[3], can damage humans' and animals' eyes and trigger nausea, vomiting, profuse sweating, and mental instability when it passes through the mouth, causing rapid or difficult breathing within short periods of inhaling.[4] Therefore, it is practically essential to remove MB from dye wastewater.

Many advanced techniques have been developed for removing MB, including the Fenton process and combined electrochemical treatments, electrochemical degradation, reverse osmosis, photodecomposition, coagulation/flocculation, membrane processing, oxidative degradation, electrocoagulation, and carbonaceous nanomaterials.[5–13] In addition, activated carbon has been recognized to effectively remove different dye molecules.[14–16] However, these methods are costly, owing to poor regeneration. In recent years, considerable efforts have been made in developing adsorbents derived from plant materials such as mango peels, pistachio shell, cladodes of *Opuntia ficus indica*, peach stone, carbonized watermelon, seed fibers, and potato peels.[17–23]

Some recent studies have used raw materials or raw materials modified with NaOH to treat MB.[26,27] For instance, plant materials modified with citric acid (CA) show good potential for wastewater treatment.[20,28,29] Cellulose fibrils extracted from *P. australis* and treated by both NaOH and CA appear to be a better-modified material compared to being treated with only NaOH as described in the previous report.[26] *P. australis* is a type of reed that mainly grows around lakes, rivers, streams, and brackish water worldwide between 10° and 70° northern latitudes.[24] This plant type has a high tissue porosity formed by cellulose, hemicellulose, and lignin, which are vital constituents for developing adsorbents.[25] It wildly grows all year round throughout the country of Viet Nam, especially in

wetlands. In this study, the biomass of *P. australis* modified with NaOH and followed by esterification using citric acid (NaOH-then-CA treatment) was investigated in adsorbing MB from aqueous solutions. In addition, the effects of environmental parameters on MB adsorption by raw and modified adsorbents were evaluated.

2. Materials and Methods

2. 1. Chemicals and Materials

Citric acid ($HOC(COOH)(CH_2COOH)_2$, ≥ 99.5%), sodium hypophosphite monohydrate ($NaH_2PO_2.H_2O$, ≥ 99.5%), sodium hydroxide (NaOH, ≥ 97%), hydrochloric acid (HCl, 37%), sodium chloride (NaCl, ≥ 99.5%), and MB ($C_{16}H_{18}N_3SCl$, 99.5%) were purchased from Sigma-Aldrich. Then, MB was diluted with double-distilled water to a range of 125–300 mg/L. The pH was adjusted using NaOH (0.1 M) and HCl (0.1 M).

P. australis samples were collected from a wetland in Dong Thap province, Vietnam and cleaned with tap water to remove dirt and other impurities adhered to their surfaces. The plant stems were dried under the sunlight for four days prior to being finely ground to approximately 1–2 mm sizes. The obtained biomass was rinsed with distilled water and dried in a vacuum oven at 70 °C to a constant weight. The product was stored in a desiccator and used as raw *P. australis* biomass (RPB).

2. 2. Chemical Modifications of *P. australis* Biomass

RPB (5 g) was added to a 250 mL glass beaker containing 100 mL NaOH (0.5 M). The solution was stirred at 60 °C and 400 rpm using a magnetic bar for 5 h. After that, the biomass was collected and cleaned with distilled water until the pH of the solution was 7.0. The product was then dried in a vacuum oven at 60 °C for 12 h until it yielded an adsorbent. The biomass modified with NaOH was designated as S-RPB, which was further denatured with a 50 mL (0.1 M) CA solution added to a 2.0 g S-RPB. Then, $NaH_2PO_2.H_2O$ (2.65 g), used as a catalyst, was added to the solution. The biomass was collected after stirring at 60 °C and 400 rpm using a magnetic bar for 5 h. After that, it was soaked in 50 mL distilled water several times until the pH reached 7.0, and then was dried at 60 °C for 12 h, and subsequently arriving at 140 °C for 3 h. The second modified adsorbent was designated as SA-RPB.

2. 3. Characterization of Materials

The lignocellulosic composition before and after being modified (as mentioned above) was determined according to the National Renewable Energy Laboratory (NREL) compositional analysis procedure.[30] The C, H, N, S, and O contents of the materials were analyzed using a CHNS-O Elemental Analyzer (Thermo, Flash EA1112, USA). Also, the products' XRD was performed by a MiniFlex 600 diffractometer (Rigaku, Japan) with a radiation source of Cu Kα, λ = 0.15406 nm. The scanned angle (2θ values) ranged between 5° and 80° with a step size of 0.01°. The adsorbents' surface morphology was scanned under the scanning electron microscopy (SEM) technique (FEI-SEM NOVA NanoSEM 450-USA). Meanwhile, the samples' FTIR spectra were recorded by an Infrared Affinity-1S spectrophotometer (Shimadzu) and BET was determined by N_2 adsorption–desorption isotherms at liquid nitrogen temperature (77 K) using a Quantachrome TriStar 3000 V6.07A absorption instrument.

2. 4. Determination of Point of Zero Charge (pH_{PZC})

The pH_{PZC} of the adsorbents was determined using the pH drift method described in a previous study.[31] Forty-five milliliters of 0.5 M NaCl with pH values were adjusted from 2 to 12 by either 0.1 M NaOH or 0.1 M HCl solution. Then, distilled water (50 mL) was added, and the pH values were readjusted, closely noting the initial pH (pH_i). Next, an obtained adsorbent was added to each flask at 1.0 g/L, incubated at 180 rpm using a magnetic stir bar for 24 h at room temperature (~30 °C). The differences in the pH (ΔpH) values between the initial pH and final pH (pH_f) ($\Delta pH = pH_i - pH_f$) were plotted against pH_i. The points of intersection of the curve with the abscissa at which ΔpH is equal to zero were presented as the pH_{PZC}.

2. 5. Adsorption Tests

Adsorption tests were performed by adding an adsorbent into a 250 mL glass beaker containing 100 mL MB solution. For the effects of the adsorbent on adsorption, the MB was diluted to 125–300 mg/L, while SA-RPB was used from 0.4 to1.4 g/L. The solution was stirred at 300 rpm, and liquid media were collected from 2 to 105 min. Liquid media samples were centrifuged at 3000 rpm for 5 min to remove solid particles. Also, MB concentrations were measured by an ultraviolet–visual spectrophotometer (Spectro UV–2650, Labomed, USA) at a wavelength of 665 nm. The percent removal (R) and adsorption capacity per unit mass (q_t) after a specific contact time (t) were calculated via Eqs. (1) and (2), respectively, as follows:

$$R(\%) = \frac{C_0 - C_t}{C_0} \times 100 \quad (1)$$

$$q_t = \frac{(C_0 - C_t) \times V}{m} \quad (2)$$

where C_0 (mg/L) and C_t (mg/L) are MB concentrations in liquid media at the initial and time t, respectively, and V is the volume of the solution (L).

2. 5. 1. Adsorption Kinetics

The adsorption kinetics were fitted to the pseudo-first-order and pseudo-second-order kinetic models, which are expressed by Eqs. (3) and (4), respectively[32,22], below:

$$q_t = q_e(1 - e^{-k_1 t}) \quad (3)$$

$$q_t = \frac{q_e^2 k_2 t}{1 + q_e k_2 t} \quad (4)$$

where k_1 (1/min) and k_2 (1/min) are rate constants of the pseudo-first-order and pseudo-second-order, respectively; and t (min) is the contact time.

2. 5. 2. Adsorption Mechanisms

The Weber–Morris intra-particle diffusion and Boyd models were applied in order to investigate diffusion mechanisms. The former model was derived from the Fick's second law of diffusion as expressed by Eqs. (5):[1,4]

$$q_t = k_{pi} t^{1/2} + C_i \quad 5)$$

where k_{pi} (mg/gmin$^{1/2}$) means the diffusion rate constant at stage i, and C_i is the intercept which can be evaluated from the slope of the linear plot of q_t versus $t^{1/2}$. The q_t (mg/g) is adsorption capacity per unit weight of adsorbent per time, and $t^{1/2}$ (min$^{1/2}$) denotes half adsorption time. The intercept, C_i, relates to the extent of external mass transfer during the adsorption, acting as the rate-controlling step. When the linear plot of q_t versus $t^{1/2}$ passes through the origin, intra-particle diffusion is the sole rate-limiting step. However, if the linear plots at each concentration do not pass through the origin, when it indicates that the intra-particle diffusion was not only rate controlling step.[1]

Meanwhile, the Boyd model was implemented to distinguish between film diffusion and intra-particle diffusion as expressed by Eqs. (6) and (7):[15,16]

$$B_t = -0.4977 - \ln(1 - F) \quad (\text{for } F > 0.85) \quad (6)$$

$$B_t = \left(\sqrt{\pi} - \sqrt{\pi - (\frac{\pi^2 F}{3})} \right)^2 \quad (\text{for } F < 0.85) \quad (7)$$

where B_t is a mathematical function of F representing the fractional attainment of equilibrium at any time t given by Eqs.(8):

$$F = \frac{q_t}{q_e} \quad (8)$$

The plot Bt versus time t (s) is used to anticipate the diffusion limit. If the plot is linear and passes through the origin, it indicates that the pore diffusion occurs. If the lines are linear and pass through the origin, the intra-particle diffusion takes place. However, if the lines are linear but do not pass through the origin or non-linear, the film diffusion controls the adsorption process.

2. 5. 3. Adsorption Isotherms

Four isotherm equations, namely the Langmuir, Freundlich, Temkin, and Dubinin–Radushkevich, were used to fit the experimental equilibrium isotherm data for MB adsorption on SA-RPB. Adsorption isotherm tests were performed by adding 0.1 g SA-RPB into 100 mL MB at a concentration range of 125–300 mg/L. The initial pH of the MB solution was 6.5, and the controlled temperatures were 30 °C (303 K). The Langmuir model assumes that adsorption is localized on a monolayer, and all adsorption sites on the adsorbent homogeneously possess the same adsorption capacity, as expressed by Eqs. (9)[35]:

$$q_e = \frac{q_{max} K_L C_e}{1 + K_L C_e} \quad (9)$$

where C_e (mg/L) is the equilibrium concentration; q_e (mg/L) is the amount of adsorbed dye at equilibrium; q_{max} (mg/g) is the maximum adsorption capacity; and K_L (L/mg) is the Langmuir adsorption equilibrium constant. The equilibrium parameter (R_L) is a dimensionless constant of the Langmuir isotherm, expressed by Eqs. (10) [35]:

$$R_L = \frac{1}{1 + K_L C_0} \quad (10)$$

where C_0 is the highest initial solute concentration. The Freundlich isotherm model assumes that multilayer adsorption processes occur on heterogeneous surfaces, expressed by Eqs. (11)[36]:

$$q_e = K_F C_e^{1/n_F} \quad (11)$$

where K_F (mg/g.(L/mg)$^{1/n}$) and n are Freundlich constants related to the adsorption capacity and adsorption intensity, respectively. The adsorbate–adsorbate interactions can cause a decrease in the heat of adsorption of all the molecules in the layer. The Temkin isotherm reflects the effect of the adsorbate interaction on SA-RPB, expressed by Eqs. (12)[37]:

$$q_e = (RT / b) \ln(A_T C_e) \quad (12)$$

$$B_T = RT / b \quad (13)$$

where A_t (L/g) and b (g.J/mg.mol) are Temkin's isotherm constants; R (8.314 J/mol.K) is the universal gas constant; T (K) is the absolute temperature. The Dubinin–Radushkevich isotherm model[38] was used to determine the mean free energy of biosorption, expressed by Eqs. (14)–(16):

$$q_e = q_{DR} e^{-K_{DR} \varepsilon^2} \quad (14)$$

$$E = 1/\sqrt{2K_{DR}} \quad (15)$$

$$\varepsilon = RT \ln(1 + \frac{1}{C_e}) \quad (16)$$

where K_{DR} is a constant related to the adsorption energy (mol^2/kJ^2); q_{DR} (mg/g) is the Dubinin–Radushkevich iso-

therm adsorption capacity; ε (kJ/mol) is the Polanyi potential; R is the ideal gas constant; and T (K) is the temperature. The free energy of adsorption (E) is considered as either chemical adsorption (E = 8–16 kJ/mol) or physical adsorption (E < 8 kJ/mol).

2. 5. 4. Adsorption Thermodynamics

The thermodynamic parameters for MB adsorption onto SA-RPB were evaluated at 303, 313, and 323 K. The Gibb's free energy change (ΔG°), enthalpy (ΔH°), and entropy (ΔS°) were calculated using Eqs. (17)–(19).

$$\Delta G^0 = -RT\ln K_L \quad (17)$$

$$\Delta G^0 = \Delta H^0 - T\Delta S^0 \quad (18)$$

Adding Eqs. (17) and (18) amounts to Eq. (19):

$$\ln K_L = -\frac{\Delta H^0}{RT} + \frac{\Delta S^0}{R} \quad (19)$$

where R (8.314 J/mol K) is the universal gas constant; T (K) the absolute temperature, and K_L the Langmuir equilibrium constant. The values of $\Delta H°$ and $\Delta S°$ can be calculated from the slope and intercept, respectively, of the linear plot of $\ln K_L$ versus $1/T$.

2. 6. Reusability

After each cycle of batch experiment, the SA-RPB was collected through centrifugation at 5000 rpm for 10 min. The adsorbent was first washed with absolute ethanol and then rinsed with double-distilled water three times. The adsorbent (0.1 mg) was transferred into 100 mL of the rinse media, stirred at 300 rpm for 6 hours, and collected through centrifugation at 5000 rpm for 10 min, followed by being dried for 24 h at 100 °C until its weight stayed constant.

3. Results and Discussion

3. 1. Characterization of Materials

The biomass components of *P. australis* are listed in Table 1. The components of the raw RPB were also determined in previous studies[39,40]. The cellulose content significantly increased, whereas hemicellulose and lignin contents comparatively decreased after the NaOH treatment (S-RPB) and the NaOH-then-CA treatment (SA-RPB) (Table 1). The C content in RBB (46.42%) decreased slightly, whereas the O content (45.82%) and the ratio of O to C increased slightly after NaOH-then-CA treatment (Table 1) was done. Moreover, the percentages of N, S, Si, K, and Mg significantly decreased after the treatment. Acidic and basic solutions are typically used for modifying and/or removing lignin and hemicellulose from plant biomass.[41] The treatment with NaOH resulted in the formation of hydroxyl groups on the S-RPB, which then reacted with citric acid, forming an ester linkage to introduce carboxyl groups into SA-RPB.[20]

Table 1. Chemical compositions of RPB, S-RPB, and SA-RPB

Parameter	RPB	S-RPB	SA-RPB
Lignocellulosic analysis (dry weight basis), wt%			
Cellulose (%)	43.31	66.32	71.21
Hemicellulose (%)	30.82	15.17	13.28
Lignin (%)	20.37	12.30	9.19
Elemental analysis (dry weight basis), wt%			
C (%)	46.42	45.71	45.23
O (%)	45.82	47.72	48.83
H (%)	5.910	5.610	5.720
N (%)	0.232	0.111	0.021
S (%)	0.313	0.222	0.107
O/C (mol/mol)	0.7403	0.7830	0.8097
Si (%)	1.050	0.021	–
K (%)	0.454	0.284	0.182
Mg (%)	0.601	0.322	0.110

SEM micrograph images of *P. australis* biomass before and after the NaOH-then-CA treatment were captured (Fig. 1). The raw material had a surface composed of fibrous rods (Fig. 1(a)). The surface morphology was found to transform, being affected by NaOH. The S-RPB sample retained its tubular structure, but the surface turned out to be more porous and uneven (Fig. 1(b)). The texture was also rough and irregular after being treated with CA (Fig. 1(c)). The treatment with citric acid reduces the cavities on the adsorbent surface. Citric acid clogged the carbon surface, which explains for a spotted reduction in the surface area and pore volume of the adsorbent.[42]

Table 2. Porous textural parameters of RPB, S-RPB, and SA-RPB samples

Sample	Surface area (m^2/g)	Pore volume (dm^3/g)	Average pore diameter (nm)
RPB	1.01	2.626	16.64
S-RPB	0.87	2.052	16.86
SA-RPB	0.74	1.935	15.97

The crystallographic structures of the RPB, S-RPB, and SA-RPB were analyzed using the XRD technique (Fig. 1(d)). The results indicated that all samples had two diffraction peaks at angles 2θ of 15.7° and 22.3°, corresponding to (101) and (002) planes of cellulose crystals.[43] The diffraction intensities were in the order of SA-RPB > S-RPB > RPB (Fig. 1(d)), indicating that NaOH-then-

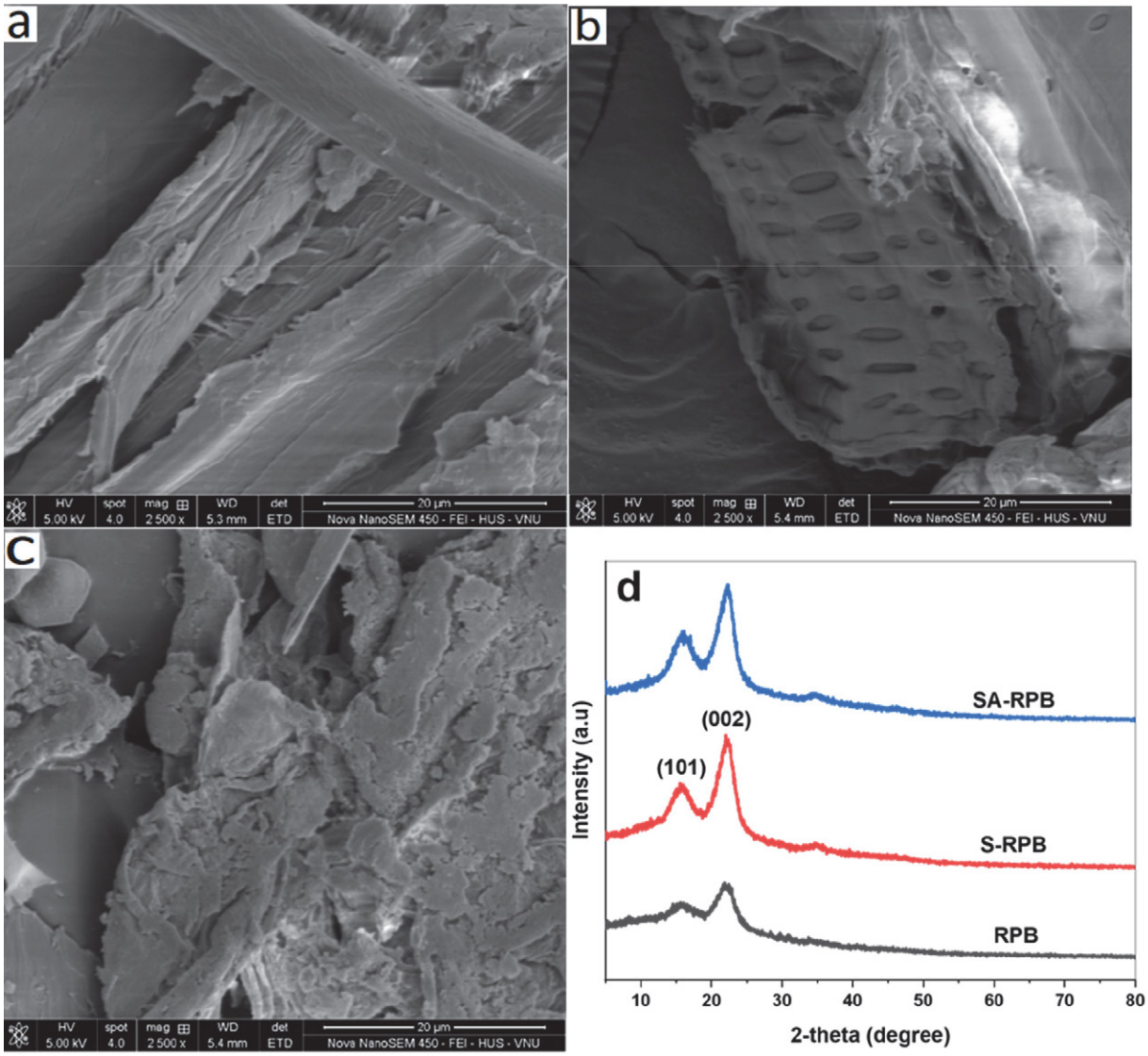

Fig. 1. Morphology and crystallization of samples; SEM images of (a) RPB, (b) S-RPB, and (c) SA-RPB; (d) XRD patterns of RPB, S-RPB, and SA-RPB samples

CA treatment enhanced the cellulose crystallinity. The increased crystallization attributed to the partial removal of amorphous polymers (hemicellulose and lignin) from plant structures has also been reported.[26,44] The specific surface area and porous texture of the obtained samples were evaluated using the nitrogen adsorption–desorption isotherms at 77 K (Table 2). The RRB sample had a specific surface area of 1.01 m^2/g, a common property of raw plant biomasses.[45] The surface areas decreased by 13.9% after the NaOH treatment and went down to 26.7%, resulting from that of the NaOH-then-CA treatment, while the pore volumes decreased by 21.8% and 26.3%. Besides, the average pore diameter slightly decreased after the treatment. Citric acid can easily penetrate the pore structure because of its small molecular size, causing the pore block of the absorbent.[42] These results indicate that the dye adsorption capacity can be boosted due to the formation of hydroxyl and carboxyl groups on the surface of *P. australis* biomass, and the functional groups might play a more important role than the surface area in MB adsorption.

The functional groups on the adsorbent surfaces with differing intensities of the observed peaks during *P. australis* biomass modification were analyzed via FTIR (Fig. 2). Adsorption bands corresponding to functional groups were determined according to Reddy.[46] A broad peak of approximately 3321 cm^{-1} corresponded to the stretching vibration of the hydroxyl groups (–OH) for cellulose, hemicellulose, and lignin, whereas the 2918 cm^{-1} band indicated the presence of C–H stretching vibrations of methyl and methylene. After the raw material was modified with NaOH and NaOH-then-CA, the stretching vibration bands of OH shifted to 3443 and 3438 cm^{-1}, respective-

ly. The band at 1734 cm^{-1} could be attributed to the C=O bond stretching of acetyl ester groups in hemicellulose, lignin, or both.

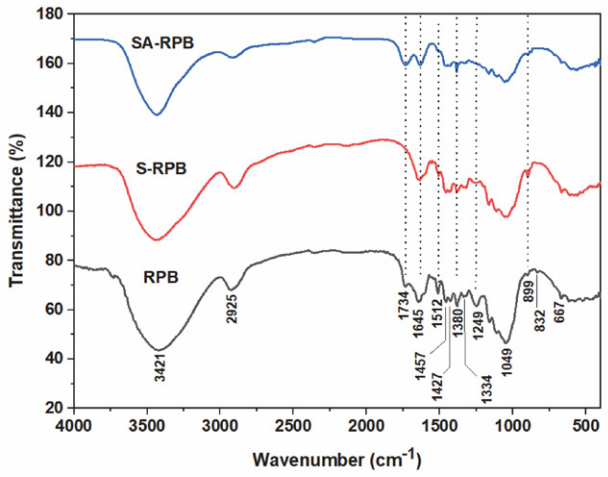

Fig. 2. FTIR spectra of RPB, S-RPB and SA-RPB samples

This adsorption peak was absent from the FTIR spectrum of the S-RPB sample (Fig. 2) after the alkaline treatment because of the removal of hemicellulose and lignin through a process called de-esterification. Moreover, C=O bond stretching was observed after the NaOH-then-CA treatment, owing to the esterification reaction. The band at 1645 cm^{-1} could be attributed to $-COO^-$ stretching of carboxylate groups with the aromatic ring. The band at approximately 1512 cm^{-1} was associated with C=C stretching vibrations in aromatic rings of lignin, whereas the band at 1427 cm^{-1} was attributed to the C–H bond deformation of lignin. The peak intensities at 1457 and 1380 cm^{-1} reflected C–H symmetric and asymmetric deformations of cellulose, respectively. The appearance of peaks at 1334 and 1327 cm^{-1} could be attributed to the –OH bending vibration in C–OH and C1–O vibrations in S derivative vibrations of cellulose, respectively. The signal at 1249 cm^{-1} corresponded to the –COO vibration of acetyl groups in hemicellulose and lignin.[20,47] The adsorption peaks at 1159 and 1111 cm^{-1} were attributed to C–O–C antisymmetric and anhydroglucose ring vibrations, respectively, whereas the band at 1049 cm^{-1} corresponded to C–O stretching vibrations of cellulose, hemicellulose, and lignin.[48] A band at 899 cm^{-1} corresponds to C–H rocking vibrations of cellulose.[49] The intensities of these parts of S-RPB and SA-RPB decreased, owing to the removal of lignin. The weak adsorption peaks of 832–400 cm^{-1} were probably related to C–H and C=H bending in aromatic rings, C–H bending, and C–O stretching.[40,50] The FTIR results indicated abundant functional groups of –OH, –COOH, and $-COO^-$ on the adsorbent surfaces.

3. 2. pH_{PZC} determination

The differences in the pH_{PZC} of RPB, S-RPB, and SA-RPB are shown in Fig. 3(a). The raw *P. australis* biomass had a pH_{PZC} of 6.72, also obtained in a previous study.[27] The pH_{PZC} levels of S-RPB and SA-RPB were 6.17 and 3.10, respectively.

The pH_{PZC} level slightly decreased after the NaOH treatment, possibly because of de-esterification and the removal of a part of hemicellulose and lignin.[51] The pH_{PZC} value of the SA-RPB was significantly lower than those of RPB and S-RPB, which could be attributed to the esterification reaction of hydroxyl on the raw material surface with the carboxyl group of citric acid to increase the carboxyl group on its surface.[20,52] Absorbents with pH values lower than pH_{PZC} absorb compounds with a positive surface charge.[53] The MB dye with a molecular diameter of 0.8 nm[54] was smaller than the pore diameter of SA-RPB (15.97 nm, Table 2); hence, MB could easily penetrate the SA-RPB pore structure. The batch adsorption test results

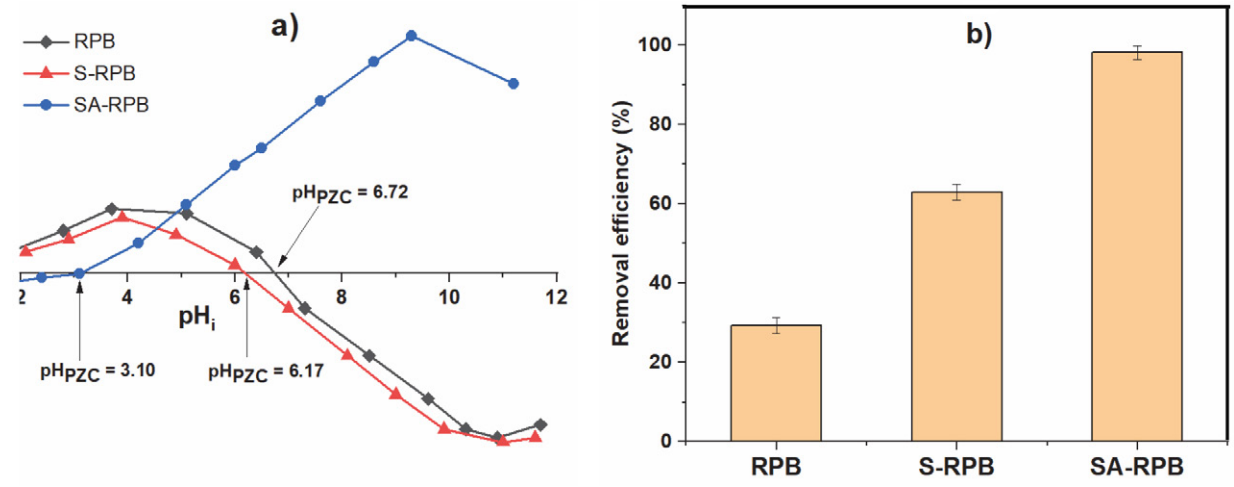

Fig. 3. (a) Plots of point of zero charges of RPB, S-RPB, and SA-RPB (1.0 g/L adsorbent at different pH values); (b) percentage removal efficiency values for MB on RPB, S-RPB, and SA-RPB samples (150 mg/L MB at 6.5 pH value)

showed that the removal efficiency by SA-RPB adsorbent was 98.11±1.76%, about 68.8 and 35.1% higher than that of RPB and S-RPB, respectively (Fig. 3(b)). The increase in removal efficiency by SA-RPB was due to both NaOH and CA modified to the raw material. Therefore, SA-RPB was used for other experiments.

3. 3. Batch Adsorption

3. 3. 1. Effect of Adsorbent Dosage

In this experiment, the effects of the adsorbent dose (SA-RPB) on MB adsorption were examined. As seen in Fig. 4, an increase in the adsorbent mass from 0.4 to 1.0 g/L improved the MB removal rate because of the increased sites available for adsorption. However, the adsorption did not statistically differ at adsorbent doses higher than 1.0 g/L. The adsorption appeared to be in equilibrium when the adsorbent mass reached a particular value, possibly because the number of MB dye molecules available in the solution was insufficient to combine with all effective adsorption sites on the adsorbent.

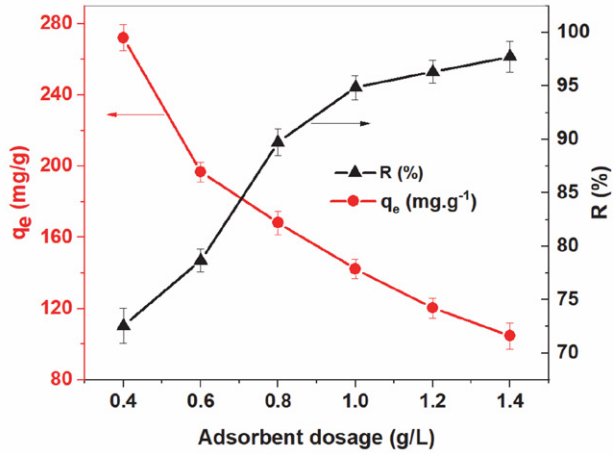

Fig. 4. SA-RPB dosage effects on equilibrium adsorption capacity (q_e, mg/g) and removal efficiency of MB (R, %) (The tests conducted for 105 min by 150 mg/L MB at 6.5 pH)

3. 3. 2. Effects of Contact Time, Temperature, and Adsorption Kinetics

The effect of contact time on MB removal via the SA-RPB adsorbent is depicted in Fig. 5. The adsorption sharply increased within 20 min at the initial stage and then attained equilibrium after 60 min at all temperatures, followed by a maximum removal. About 89.98% of equilibrium adsorption capacity was achieved within 10 min. The fast adsorption at the initial stage was probably caused by available vacant active sites of the adsorbent (with functional groups of –OH, –COOH, and –COO^-) and a higher driving force between MB ions and the surface. However, adsorption isotherms at three temperatures were not statistically different. This phenomenon is due to available active sites for adsorption, which previous studies used to modify plant materials for MB removal[55,56]. Meanwhile, decreased vacant sites and insufficient active sites of the adsorbent slowed down the adsorption rate and equilibrium.[56]

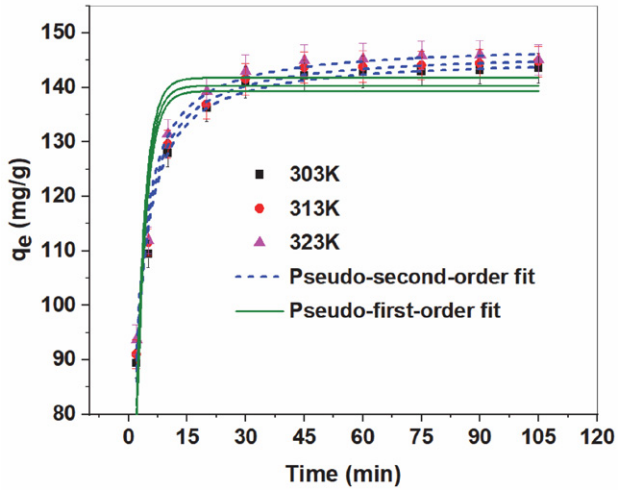

Fig. 5. Pseudo-first and pseudo-second-order kinetics for MB adsorption by SA-RPB at different temperatures. The experiments were conducted by 1.0 g/L SA-RPB and 150 mg/L MB at 6.5 pH

Two kinetic models (pseudo-first-order and pseudo-second-order) were used to determine adsorption rate and analyze kinetic data. The calculated correlation coefficients (R^2) and other data are listed in Table 3. The $q_{e,cal}$ and $q_{e,exp}$ values for each model at different temperatures slightly rose, whereas (and) k_1 and k_2 tended to increase at higher temperatures, indicating that adsorption kinetics was faster at higher temperatures. This shows that the adsorption is the endothermic, in which higher temperature is more favorable for dye adsorption.

Regarding the second-order kinetic model as seen in Table 3, it fitted well with high correlation coefficients ($R^2 > 0.98$). Moreover, slight differences between calculated data ($q_{e,cal}$) and experimental data ($q_{e,exp}$) and its low χ^2 values indicated the optimum adsorption at the equilibrium. Therefore, the model better described experimental data indicating the adsorption highly depended on available active sites more than MB concentrations. Thus, it satisfactorily simulates MB adsorption onto modified cellulose fibers of *P. australis*.[26,27]

3. 3. 3. Intra-particle Diffusion and Film Diffusion Models

Intra-particle diffusion was used to analyze kinetic adsorption at different MB concentrations. The multi-linear (Fig. 6) shows three phases of the adsorption process. The first phase occurred within first 10 min, probably due to the adsorption on external surface of the adsorbent, or

Table 3. Kinetic parameters for MB adsorption by SA-RPB at different temperatures

Temp. (K)	$q_{e,exp}$ (mg/g)	First-order kinetic model				Second-order kinetic model			
		k_1 (1/min)	$q_{e,cal}$ (mg/g)	R^2	χ^2	k_2 (1/min)	$q_{e,cal}$ (mg/g)	R^2	χ^2
303	143.56	0.4047	139.36	0.807	4.084	0.0049	145.64	0.987	0.340
313	144.75	0.4192	140.35	0.849	3.841	0.0051	146.58	0.989	0.281
323	145.11	0.4275	141.79	0.828	4.241	0.0052	147.93	0.981	0.467

boundary layer diffusion of solute molecules (film diffusion).[1,12] The electrostatic attraction between MB and the adsorbent might involve in this phase. The second phase was intra-particle diffusion at a gradual adsorption stage. The last one was equilibrium phase during which intra-particle diffusion occurred when MB concentration was reduced.

Non-zero C_i intercepts (Table 4) showed that the intra-particle diffusion was not the only rate limiting step. Moreover, the fact that the first and second phases did not pass through the origin signifies the intra-particle diffusion. C_i enhanced when the temperature increased (Table 4), indicating that temperature promoted the boundary layer diffusion effect.[1]

The boundary layer diffusion rate constants of the first phase (k_{p1}) were significantly higher than those of the second and third ones (Table 4). These results signify that mass transfer from bulk solution to exterior surface of SA-RPB was higher than that from exterior surface into its pores. Moreover, k_p value at 313 K was higher than at 303 K, boosting MB diffusion rate.

As shown in Fig. 8, calculated *Bt* values were plotted adsorption against time *t* (min). It denotes that linear lines for all MB initial concentrations did not pass through the origin. This indicates that MB adsorption on prepared SA-RPB is mainly governed by external mass transport, where particle diffusion is the rate limiting step.

Boyd model was used to distinguish between film and intra-particle diffusions. Accordingly, *Bt* values plotted against time can be used to determine diffusion processes. If the lines are linear and pass through the origin, then intra-particle diffusion occurs. However, if they are

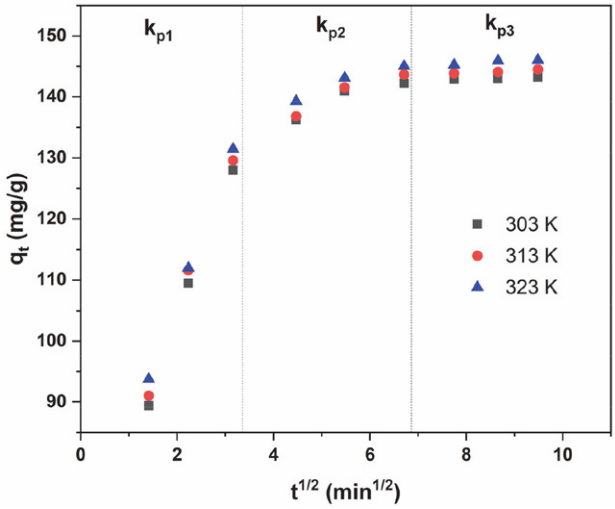

Fig. 6. Plots of intra-particle diffusion model for the adsorption of MB dye onto SA-RPB at 203; 313 and 323 K

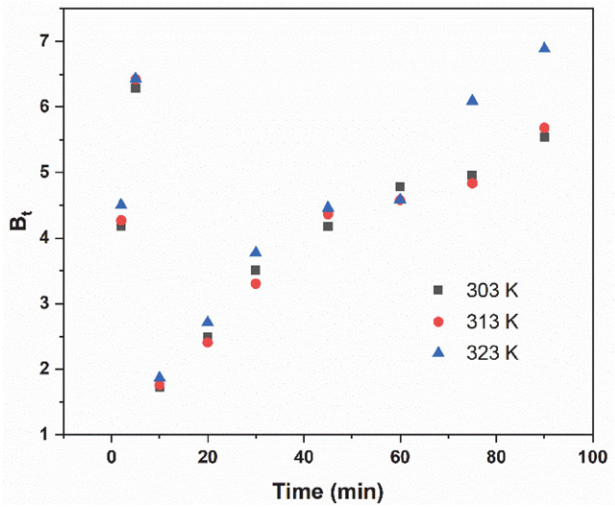

Fig. 7. Boyd plots for MB adsorption by SA-RPB at 303, 313, and 323 K

Table 4. Intra-particle diffusion model constant for MB adsorption by SA-RPB at different temperatures

Temp. (K)	Intra-particle diffusion model								
	k_{p1} (mg/gmin$^{1/2}$)	k_{p2} (mg/gmin$^{1/2}$)	k_{p3} (mg/gmin$^{1/2}$)	C_1	C_2	C_3	$(R_1)^2$	$(R_2)^2$	$(R_3)^2$
303	22.065	2.607	0.220	58.823	125.330	141.099	0.996	0.862	0.939
313	22.114	3.000	0.342	60.732	123.992	141.161	0.994	0.926	0.953
323	21.584	2.520	0.470	63.361	128.449	141.652	0.999	0.940	0.870

linear but do not pass through the origin, or non-linear, then film diffusion controls the adsorption process. [15,16] Fig. 7 shows that the Boyd plots at all temperatures are non-linear, indicating the film diffusion occurred. This probably resulted from a mass transfer difference in the first and second phases.

3. 3. 4. Effects of Initial MB Concentration and Adsorption Isotherms

The effects of initial MB concentration (from 125 to 300 mg/L) on adsorption were determined by 0.1 g/L SA-RPB, at pH 6.5 and 303 K. Adsorption isotherms were analyzed at different initial MB concentrations, reflecting MB removal by SA-RPB (Fig. 8(a)). It clearly displays that the removal rate rapidly went up from 125 to 250 mg/L MB concentrations and gradually increased at higher concentrations. More than 94% MB was absorbed at 125 and 150 mg/L concentrations, and the MB equilibrium adsorption capacity (q_e) increased with higher initial dye concentrations (Fig. 8(a)). However, the initial MB concentration (from 125 to 300 mg/L) resulted in a decreased MB removal from 96.93% to 63.64% at 303 K (Fig. 8(a)). The lack of available active sites required for high initial MB concentrations accounted for these reductions. The adsorption isotherms, which revealed the interactive behaviors between the adsorbate and adsorbent at liquid–solid interfaces, were analyzed.

The obtained results show that Langmuir, Freundlich, Dubinin–Radushkevitch, and Temkin models simulated MB adsorption on SA-RPB. The nonlinear plots at different concentrations are evident in Fig. 8(b), while Table 4 depicts their corresponding parameters. R^2 and χ^2 were used as indicators to analyze adsorption at equilibrium. Langmuir model appeared to yield the best fit because of its higher R^2 and lower χ^2 than those of other models. The Langmuir isotherm model showed the homogeneous nature of the adsorbent surface and the monolayer cover of dye molecules formed on the outer surface of SA-RPB. Also, its isotherm R_L values indicate that the fundamental features were higher than 0 and less than 1.0; thus, the adsorption was favorable within the evaluated concentration range.[57] For the Freundlich model, the 1/n values (Table 5) were within the range of $0.1 < 1/n < 1.0$, signifying physisorption mechanism, and the adsorption process was considered favorable, rapid, and effective.[58] The equilibrium models provide insights on the adsorbent's adsorption mechanism, surface properties, and affinity.

Non-linear regression of the Temkin model fitted well with the experimental data with high R^2(T) and low χ^2(T) (Table 5). B_T was 21.47 J/mol at 303K, reflecting the endothermic nature of adsorption. The R^2(DR) value generated by Dubinin–Radushkevitch isotherm (Table 5) was significantly lower than those of other isotherms mentioned above. This result shows that the MB adsorption by SA-RPB was not well-aligned with the Dubinin–Radushkevitch isotherm. Moreover, mean energy of sorption (E) calculated from this model was 0.615 kJ/mol at 303 K, which proved the endothermic nature of adsorption.[15]

The NaOH-then-CA adsorbent exhibited its effective MB removal with a maximum adsorption capacity of 191.49 mg/g at 150 mg/L MB concentration. This value is higher than those obtained in other studies using modified *P. australis* biomass and other modified plant materials listed in Table 6. For example, Kankılıç *et al.* reported that the maximum adsorption capacity of cellulose microfibrils of *P. australis* modified with NaOH was 54.9 mg/g at 400 mg/L.[58] The treatment with citric acid increased the absorption ability in our study.

3. 3. 5. Adsorption Thermodynamics

Determining thermodynamic parameters is also conducted to better understand temperature effects on

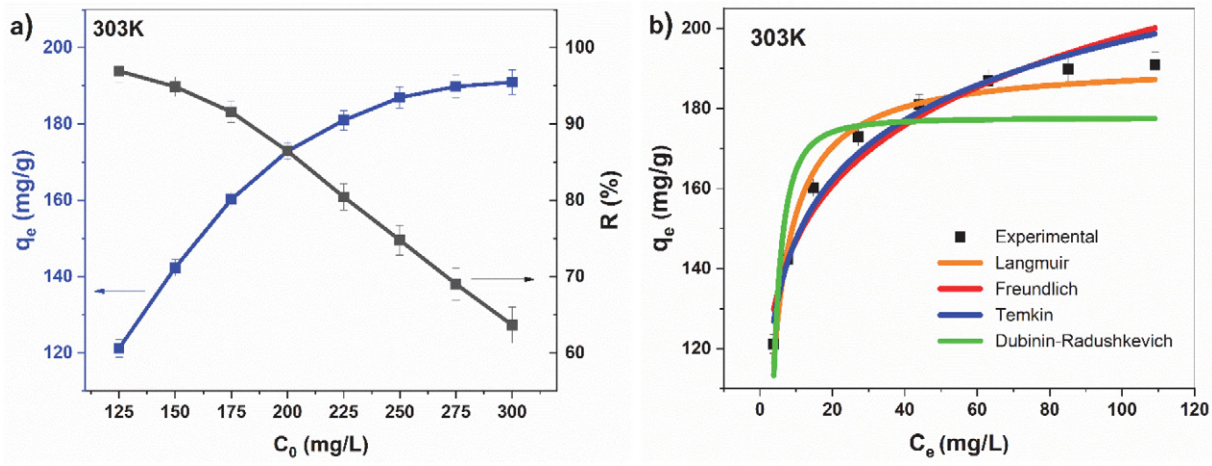

Fig. 8. (a) Effect of initial MB concentration on MB removal efficiency and adsorption capacity by SA-RPB at 303 K; (b) MB adsorption isotherm by SA-RPB based on Langmuir, Freundlich, Temkin, and Dubinin–Radushkevich isotherm models at 303 K. The experiments were conducted using 1.0 g/L SA-RPB at different initial MB concentrations and 6.5 pH value

Table 5. Isotherm parameters for MB adsorption by SA-RPB at 303K

Temp. (K)	$q_{e,exp}$ (mg/g)	Langmuir isotherm					*Freundlich* isotherm			
		q_{max} (mg/g)	K_L (L/mg)	R_L	$R^2(L)$	$\chi^2(L)$	K_F (mg/g. (L/mg)$^{1/n}$)	n_F	$R^2(F)$	$\chi^2(F)$
303	190.94	191.49	0.404	0.0082	0.981	0.548	109.15	7.739	0.946	99.505
Temp. (K)	$q_{e,exp}$ (mg/g)	**Dubinin–Radushkevitch isotherm**					**Temkin isotherm**			
		q_{DR} (mg/g)	E (kJ/mol)	K_{DR} (mol^2/kJ^2)	$R^2(DR)$	$\chi^2(DR)$	A_T (L/mg)	B_T (J/mol)	$R^2(T)$	$\chi^2(T)$
303	190.94	177.62	0.615	-1.32×10^{-6}	0.817	5.135	95.66	21.47	0.970	0.867

Table 6. MB adsorbents' capacities in comparison

Absorbent	Temperature (K)	pH	q_{max} (mg/g)
P. australis treated with NaOH and citric acid	303	6.5	191.49
P. australis treated with NaOH[26]	298	7.0	54.9
Raw *P. australis*[58]	298	6.5	22.7
P. australis treated with organic compounds[58]	298	6.5	46.8
Raw Tunisian *P. australis*[27]	298	8.0	41.2
Peach stones modified with citric acid[20]	303	6.0	178.25
Lawny grass treated with citric acid[28]	298	5.7	301.1
Peanut shell modified with citric acid[29]	303	10.0	120.48
Activated carbon[15]	303	7	81.20

adsorption processes, applying Arrhenius equation (Eqs. (20)). Accordingly, a chemical reaction velocity is used for all predictive expressions of reaction-rate constants.

$$\ln k_2 = \ln A - \frac{E_a}{RT} \quad (20)$$

In Eqs. (20), A (g/mg·min) is the pre-exponential factor; E_a (kJ/mol) is the activation energy of absorption; R (8.314 J/mol K) is the gas constant, and T (K) is absolute temperature.

Plots of $\ln K_2$ versus $1/T$ and $\ln K_L$ versus $1/T$ were straight lines with R^2 values of 0.99 and 0.98, respectively, from which E_a and A values were calculated (Table 7). The low values of activation energy (< 42 kJ/mol) obtained in this study indicated a diffusion-controlled process and a physisorption mechanism.[59] The negative values of $\Delta G°$ at all temperatures reveal that the adsorption process was feasible and spontaneous. The obtained $\Delta S°$ was positive, showing the endothermic nature of adsorption, while the positive $\Delta S°$ spotted an increased randomness of the solid–liquid and adsorption medium interface over the process. The positive $\Delta S°$ value also indicated the adsorbent's affinity and some structural changes in adsorbate and adsorbent.[60]

3. 3. 6. Effect of Initial pH

An increase in pH from 1.0 to 6.5 significantly enhanced adsorption, but adsorption rates stayed almost constant at a higher pH value (Fig. 9). The adsorbent surface got more positively charged at low pH values, reducing the attraction between the adsorbent and MB. A more negatively charged surface is available when pH increases, facilitating greater MB uptake.[51] The pH effect on MB removal efficiency could be attributed to functional groups' features on the surface and isoelectric point pH_{PZC} of the SA-RPB adsorbent. The isoelectric point pH_{PZC} value of SA-RPB (determined by the drift pH method) was 3.1 (as seen in Fig. 3(a) above). The hydroxyl (–OH) and carboxyl (–COOH) groups were dominant on SA-RPB surface, which was deprotonated and became less charged, i.e. $pH_{PZC} < 3.1$.[61] When initial pH (pH_{in}) was lower than pH_{PZC} (3.1), the adsorbent surface was protonated and became more positive.[61] In this case, the SA-RPB surface exhibited an electrostatic repulsion between SA-RPB surface and the MB–N^+ cation in the solution, leading to poor adsorption efficiency.[62] In contrast, when pH value was lower than pH_{PZC}, functional groups on SA-RPB surface were depro-

Table 7. Thermodynamic parameters for MB adsorption by SA-RPB

E_a (kJ/mol)	A (g/mg min)	Temperature (K)	$\Delta G°$ (kJ/mol)	$\Delta H°$ (kJ/mol)	$\Delta S°$ (kJ/mol K)
2.242	0.012	303	–28.63	16.82	0.155
		313	–30.18		
		323	–31.73		

tonated and became more negative, inducing electrostatic attraction to MB–N^+ and boosting the removal efficiency.[62]

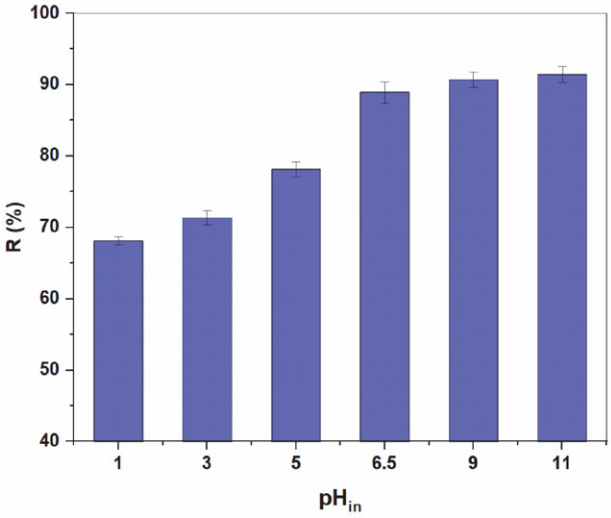

Fig. 9. Initial pH effects on MB adsorption by SA-RPB (The tests performed using 1.0 g/L SA-RPB at 150 mg/L MB concentration)

3. 3. 7. Possible Mechanism of MB Adsorption onto SA-RPB

Dye adsorption involves adsorbent-adsorbate interactions in the solution. Based on the result ($\Delta H°$ = 16.82 kJ/mol), adsorption was mainly induced by electrostatic and/or hydrogen bond forces.[63] At a pH < 3.1 (pH_{PZC} of SA-RPB), the protonated adsorbent surface became positively charged (Fig. 3(a)). Therefore, the MB–N^+ adsorption was mainly attributed to physical interaction caused by capillary diffusion and weak hydrogen bonds. The surface of negatively charged adsorbent electrostatically interacted with MB–N^+ at pH > 3.1, improving MB adsorption efficiency by SA-RPB, which reached a maximum value at the initial pH of the MB solution (6.5); hence, this pH value was selected to evaluate the adsorption mechanism.

The FTIR analysis plots showed the spectra of MB, SA-RPB, and SA-RPB after MB adsorption and were used to describe their adsorption mechanisms. From the spectral peaks (Fig. 10), vibrations were revealed (Table 8). Based on the wavenumbers, it implies that pure MB had functional groups, that is, –OH, C=C, C=N, C=N^+, C–N, C=S, C–S, and C–H.[64,65] Variations in functional groups' peak positions and the strength of SA-RPB dye complex indicate MB adsorption onto the SA-RPB surface. Differences in the wavenumbers for C–H deformation in the benzene ring, C–N in the heterocycle, and C–N bonds connected with the benzene ring in the MB, C–H aromatic rings, C=C stretching vibrations in aromatic rings, and C–H asymmetric deformation in SA-RPB and SA-RPB dye complex (Table 8) corresponded to MB attachment to the adsorbent surface by π–π stacking between the aromatic backbone of MB and SA-RPB.[50,64] This interaction was evidently reflected by adsorption peaks of MB and SA-RPB at 1599 and 1506 cm^{-1}, respectively, disappearing in SA-RPB dye complex. Furthermore, SA-RPB peak at 897 cm^{-1} after MB adsorption (Fig. 10), attributed to the bending vibration of C–H in the aromatic ring, moved up to a higher intensity than the SA-RPB sample before MB adsorption.

The peak ranges of 1340–1000 cm^{-1} of SA-RPB with oxygen-rich functional groups shifted, suggesting hydrogen bonds created between SA-RPB and MB molecules. The band shifts occurred as N–CH_3 stretching, Ar–N deformation vibration, C=S stretching vibration, and C–S stretching vibration. These phenomena signify that N in the –$N(CH_3)_2$ and Ar–N groups and S in the C=S and C–S groups might have been used as the hydrogen-bonding acceptor and formed intramolecular hydrogen bonding with the hydrogen atom of the –OH and –COOH groups on the adsorbent surface.[64] Hydrogen atoms in SA-RPB functional groups could also generate hydrogen bonds with N and S in MB functional groups. In addition, SA-RPB dye complex had a new adsorption peak at 1249 cm^{-1}, owing to the Ar–N deformation vibration of the MB molecule; this verified MB adsorption onto the SA-RPB surface.

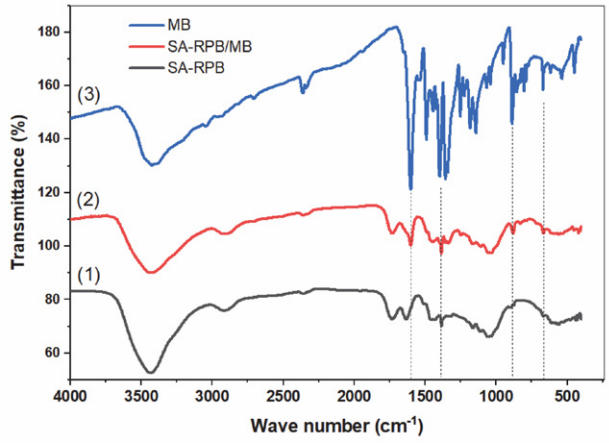

Fig. 10. FTIR spectra of SA-RPB (1) before and (2) after MB adsorption, and (3) pure MB

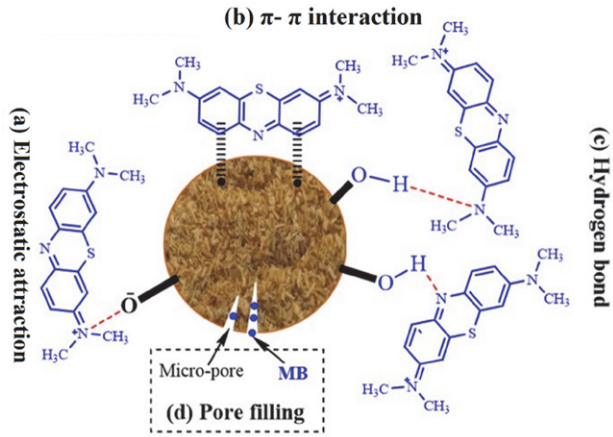

Fig. 11. Possible adsorption mechanism of MB onto SA-RPB

Table 8. FTIR spectral features of MB and SA-RPB before and after MB adsorption

MB		SA-RPB		
Vibration (cm^{-1})	Wavenumber (cm^{-1})		Vibration	Wavenumber
			Before ads.	After ads.
O–H or N–H stretching	3424	–OH stretching	3438	3427
$–CH_3$ stretching	2939	C–H stretching vibration	2917	2915
C=N–C group	2360	–COOH stretching vibration	1735	1734
$=N^+(CH_3)_2$ stretching	1661	$–COO^-$ stretching of carboxylate groups with an aromatic ring	1633	1601
C=N (and C=C) stretching in heterocycle	1599	C=C stretching vibrations in aromatic rings	1506	–
C–H deformation in benzene ring	1492	C–H deformation in aromatic rings	1456	1489
C–N in heterocycle	1396	C=C stretching vibrations in aromatic rings	1431	1447
C–N bonds connected with benzene ring	1356	C–H asymmetric deformation	1384	1385
$N–CH_3$ stretching	1340	–OH bending vibration in C–OH	1334	1355
		C1–O vibrations in S derivatives	1321	1335
Ar–N deformation vibration	1252		–	1249
C=S stretching vibration	1183	C–O–C antisymmetric vibrations	1165	1164
C–S stretching vibration	1142	Anhydroglucose ring vibration	1111	1109
C–N stretching vibration	1066; 1038	C–O stretching vibration in cellulose, hemicellulose, and lignin	1057; 1035	1056; 1034
C–H axial deformation in aromataic rings	950–669	C–H rocking vibrations	898	897
C–S and C–N stretching	616–449	C–H bending in aromatic rings	875–500	875–500

These obtained results clearly show that MB adsorption by SA-RPB was attributed to four possible adsorption mechanisms: electrostatic interaction, hydrogen bonding, π–π stacking interaction, and pores filling between MB and SA-RPB (Fig. 11) (i.e., adsorbent-adsorbate interactions).

3. 4. Reusability

The reusable efficiency of adsorbents for wastewater treatment is economically and environmentally critical. The regeneration results showed that the adsorption efficiency decreased by approximately 11.69% after six desorption–adsorption cycles compared with the first batch experiment (Fig. 12(a)). Ethanol was used to desorption MB from adsorbents in some previous reports.[66,67] Additionally, FTIR spectra of adsorbents showed similar spectra after six cycles (Fig. 12(b)), indicating the adsorbent stability during the adsorption process. This result suggests that the adsorbent is practically useful for treating real-time industrial effluent.

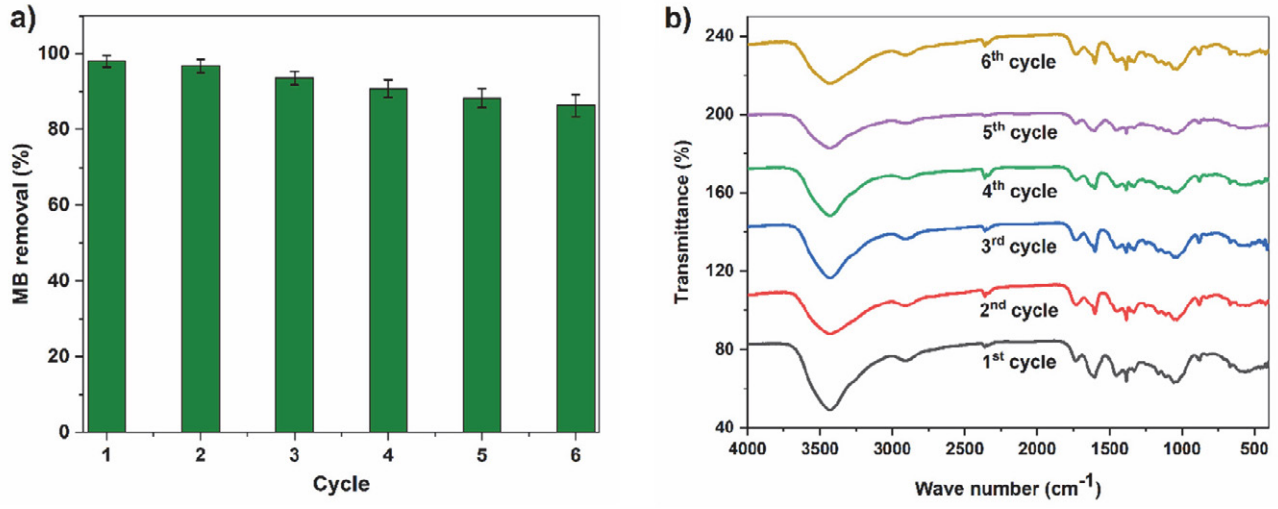

Fig. 12. (a) Removal efficiency of MB onto SA-RPB in successive desorption–adsorption cycles; (b) FTIR spectra of SA-RPB after six desorption–absorption cycles. The tests were done using 1.0 g/L SA-RPB at 150 mg/L MB concentration and 6.5 pH

4. Conclusion

This study demonstrates that chemically modified *P. australis* biomass can be used as an effective adsorbent for removing MB dye from aqueous solutions. Batch adsorption test results show that materials treated with NaOH followed by citric acid boosted the removal compared with raw materials or those modified with only NaOH. The initial pH of the solution, the adsorbent dosage, contact time, and initial MB concentrations significantly influenced the adsorption rates of SA-RPB. All SEM, FTIR, and BET analyses indicate significant modifications in the structure after chemical treatments. Moreover, calculated adsorption energy denotes that MB adsorption by SA-RPB occurred through physical interactions at different temperatures when the removal process was endothermic and spontaneous. The maximum MB adsorption capacity of SA-RPB was 191.49 mg/g, which was slightly decreased after four desorption–adsorption cycles. Four possible adsorption mechanisms (i.e., electrostatic interaction, hydrogen bonding, π–π stacking interaction, and pores filling between MB and SA-RPB) were spotted to functionally take place. This study shows that modified materials derived from reeds are expected to be highly economical and efficient for removing synthetic dyes in wastewater treatment. For practical uses, column experiments are underway for viable industrial scales and will be presented in the future.

Acknowledgements

This research is supported by the project SPD2020. 01.05. The authors are thankful to Dong Thap University for providing the instrumental facility and financial support.

Competing interests

The authors declare that no conflict of interest would prejudice the impartiality of this scientific work.

5. References

1. Y. Yao, F. Xu, M. Chen, Z. Xu, Z. Zhu, *Bioresour. Technol.* **2010**, *101*(9), 3040–3046. **DOI:**10.1016/j.biortech.2009.12.042
2. L. Meili, P. V. S. Lins, M. T. Costa, R. L. Almeida, A. K. S. Abud, J. I. Soletti, G. L. Dotto, E. H. Tanabe, L. Sellaoui, S. H. V. Carvalho, A. Erto, *Prog. Biophys. Mol. Biol.* **2019**, *141*, 60–71. **DOI:**10.1016/j.pbiomolbio.2018.07.011
3. N. Nasuha, B. H. Hameed, A. T. Din, *J. Hazard. Mater.* **2010**, *175*(1-3), 126–132. **DOI:**10.1016/j.jhazmat.2009.09.138
4. M. J. Ahmed, S. K. Dhedan, *Fluid Phase Equilibria* **2012**, *317*, 9–14. **DOI:**10.1016/j.fluid.2011.12.026
5. A. Lahkimi, M. A. Oturan, N. Oturan, M. Chaouch, *Environ. Chem. Lett.* **2006**, *5*(1), 35–39. **DOI:**10.1007/s10311-006-0058-x
6. M. Panizza, A. Barbucci, R. Ricotti, G. Cerisola, *Sep. Purif. Technol.* **2007**, *54*(3), 382–387. **DOI:**10.1016/j.seppur.2006.10.010
7. S. K. Nataraj, K. M. Hosamani, T. M. Aminabhavi, *Desalination* **2009**, *249*(1), 12–17. **DOI:**10.1016/j.desal.2009.06.008
8. F. Gulshan, S. Yanagida, Y. Kameshima, T. Isobe, A. Nakajima, K. Okada, *Water Res.* **2010**, *44*(9), 2876–2884. **DOI:**10.1016/j.watres.2010.01.040
9. K. L. Yeap, T. T. Teng, B. T. Poh, N. Morad, K. E. Lee, *Chem. Eng. Sci.* **2014**, *243*, 305–314. **DOI:**10.1016/j.cej.2014.01.004
10. M. Soniya, G. Muthuraman, *Ind. Eng. Chem.* **2015**, *30*, 266–273. **DOI:**10.1016/j.jiec.2015.05.032
11. M. Khaksar, D. M. Boghaei, M. Amini, *Comptes. Rendus. Chimie.* **2015**, *18*(2), 199–203. **DOI:**10.1016/j.crci.2014.04.004
12. M. K. Mbacké, C. Kane, N. O. Diallo, C. M. Diop, F. Chauvet, M. Comtat, T. Tzedakis, *J. Environ. Chem. Eng.* **2016**, *4*(4), 4001–4011. **DOI:**10.1016/j.jece.2016.09.002
13. W. Ahlawat, N. Kataria, N. Dilbaghi, A. A. Hassan, S. Kumar, K. H. Kim, *Environ. Res.* **2020**, *181*, 108904. **DOI:**10.1016/j.envres.2019.108904
14. N. H. Thang, D. S. Khang, T. D. Hai, D. T. Nga, P. D. Tuan, *RSC Advances* **2021**, *11*(43), 26563–26570. **DOI:**10.1039/D1RA04672A
15. M. F. M. Yusop, M. A. Ahmad, N. A. Rosli, M. E. A. Manaf, *Arab. J. Chem.* **2021**, *14*(6), 103122. **DOI:**10.1016/j.arabjc.2021.103122
16. F. Marrakchi, M. J. Ahmed, W. A. Khanday, M. Asif, B. H. Hameed, *Int. J. Biol. Macromol.* **2017**, *98*, 233–239. **DOI:**10.1016/j.ijbiomac.2017.01.119
17. A. H. Jawad, N. F. Hanani Mamat, M. Fauzi Abdullah, K. Ismail, *Desalin. Water Treat.* **2016**, *59*, 210–219. **DOI:**10.5004/dwt.2017.0097
18. **İ**. Şentürk and M. Alzein, *Acta Chim. Slov.* **2020**, *67*, 55–69. **DOI:**10.17344/acsi.2019.5195
19. B. Djobbi, G. L. B. Miled, H. Raddadi and R. B. Hassen, Alzein, *Acta Chim. Slov.* **2021**, 68, 548-561. **DOI:**10.17344/acsi.2020.6248
20. J. Yan, G. Lan, H. Qiu, C. Chen, Y. Liu, G. Du, J. Zhang, *Sep. Sci. Technol.* **2018**, *53*(11), 1678–1688. **DOI:**10.1080/01496395.2018.1439064
21. A. H. Jawad, R. Razuan, J. N. Appaturi, L. D. Wilson, *Surf. Interfaces* **2019**, *16*, 76–84. **DOI:**10.1016/j.surfin.2019.04.012
22. N. Sebeia, M. Jabli, A. Ghith, Y. El Ghoul, F. M. Alminderej, *Int. J. Biol. Macromol.* **2019**, *121*, 655–665. **DOI:**10.1016/j.ijbiomac.2018.10.070
23. K. Ben Jeddou, F. Bouaziz, F. Ben Taheur, O. Nouri-Ellouz, R. Ellouz-Ghorbel, S. Ellouz-Chaabouni, *Water Sci. Technol.* **2021**, *83*(6), 1384–1398. **DOI:**10.2166/wst.2021.075
24. A. I. Engloner, *Morphol.* **2009**, *204*(5), 331–346. **DOI:**10.1016/j.flora.2008.05.001
25. T. Březinová, J. Vymazal, *Ecol. Eng.* 2014, *73*, 53–57. **DOI:**10.1016/j.ecoleng.2014.09.022
26. G. B. Kankılıç, A. Ü. Metin, *J. Mol. Liq.* **2020**, *312*, 113313. **DOI:**10.1016/j.molliq.2020.113313
27. R. Dallel, A. Kesraoui, M. Seffen, *J. Environ. Chem. Eng.* **2018**,

6(6), 7247–7256. **DOI:**10.1016/j.jece.2018.10.024
28. L. Chen, A. Ramadan, L. Lü, W. Shao, F. Luo, J. Chen, *J. Chem. Eng. Data.* **2011**, *56*(8), 3392–3399. **DOI:**10.1021/je200366n
29. P. Wang, Q. Ma, D. Hu, L. Wang, *Water Treat.* **2015**, *57*(22), 10261–10269. **DOI:**10.1080/19443994.2015.1033651
30. A. Sluiter, B. Hames, R. Ruiz, C. Scarlata, J. Sluiter, D. Templeton, D. Crocker, National Renewable Energy Laboratory Golden Co., **2008**.
31. M. Danish, T. Ahmad, S. Majeed, M. Ahmad, L. Ziyang, Z. Pin, S. M. Shakeel Iqubal*Bioresour. Technol. Rep.* **2018**, *3*, 127–137. **DOI:**10.1016/j.biteb.2018.07.007
32. S. Lagergren, *Handlingar Band,* **189**8, *24*(4), 1–39.
33. Y. S. Ho, G. McKay, *Process Biochem.* **1999**, *34*, 451–465. **DOI:**10.1016/S0032-9592(98)00112-5
34. L. Mouni, L. Belkhiri, J.-C. Bollinger, A. Bouzaza, A. Assadi, A. Tirri, F. Dahmoune, K. Madani, H. Reminie, *Appl. Clay Sci.* **2018**, *153*, 38–45. **DOI:**10.1016/j.clay.2017.11.034
35. K. R. Hall, L. C. Eagleton, A. Acrivos, T. Vermeulen, *Ind. Eng. Chem. Fundam.* **1966**, *5*(2), 212–223. **DOI:**10.1021/i160018a011
36. H. M. Freundlich, *J. Phys. Chem. A.* **1906**, *57*, 385–470. **DOI:**10.1515/zpch-1907-5723
37. M. J. Temkin, V. Pyzhev, *URSS.* **1940**, *12*, 217–225.
38. M. M. Dubinin, L. V. Radushkevich, *Proceedings of the Academy of Sciences of the USSR.* **1947**, *55*, 331–337.
39. H. Zhao, H. Yan, C. Zhang, X. Liu, Y. Xue, Y. Qiao, Y. Tian, S. Qin, *Evid. Based Complement Alternat. Med.* **2011**, 408973. **DOI:**10.1155/2011/408973
40. A. El Shahawy, G. Heikal, *Ecol. Eng.* **2018**, *122*, 207–218. **DOI:**10.1016/j.ecoleng.2018.08.004
41. D. D. Q. Melo, V. D. O. S. Neto, F. C. D. F. Barros, G. S. C. Raulino, C. B. Vidal, R. F. do Nascimento, *J. Appl. Polym. Sci.* **2016**, *133*(15), 43286. **DOI:**10.1002/app.43286
42. J. P. Chen, S. Wu, K.-H. Chong, *Carbon.* **2003**, *41*(10), 1979–1986. **DOI:**10.1016/S0008-6223(03)00197-0
43. P. Lu, Y. L. Hsieh, *ACS Appl. Mater. Interfaces.* **2010**, *2*(8), 2413–2420. **DOI:**10.1021/am1004128
44. D.-Y. Kim, B. -M. Lee, D. H. Koo, P. -H. Kang, J. -P. Jeun, *Cellulose* **2016**, *23*(5), 3039–3049. **DOI:**10.1007/s10570-016-1037-4
45. A. Barakat, C. Mayer-Laigle, A. Solhy, R. A. D. Arancon, H. de Vries, R. Luque, *RSC Adv.* **2014**, *4*(89), 48109–48127. **DOI:**10.1039/C4RA07568D
46. K. O. Reddy, B. R. Guduri, A. V. Rajulu, *J. Appl. Polym. Sci.* **2009**, *114*(1), 603–611. **DOI:**10.1002/app.30584
47. C. Uma Maheswari, K. Obi Reddy, E. Muzenda, B. R. Guduri, A. Varada Rajulu, *Biomass and Bioenergy* **2012**, *46*, 555–563. **DOI:**10.1016/j.biombioe.2012.06.039
48. C. Pappas, P. A. Tarantilis, I. Daliani, T. Mavromustakos, M. Polissiou, *Ultrason. Sonochem.* **2002**, *9*(1), 19–23. **DOI:**10.1016/S1350-4177(01)00095-5
49. A. Alemdar, M. Sain, *Bioresour Technol.* **2008**, *99*(6), 1664–1671. **DOI:**10.1016/j.biortech.2007.04.029
50. L. Hevira, Zilfa, Rahmayeni, J. O. Ighalo, H. Aziz, R. Zein, *J. Ind. Eng. Chem.* **2021**, *97*, 188–199. **DOI:**10.1016/j.jiec.2021.01.028
51. D. H. K. Reddy, Y. Harinath, K. Seshaiah, A. V. R. Reddy, *Chem. Eng. Sci.* **2010**, *162*, 626–634. **DOI:**10.1016/j.cej.2010.06.010
52. H. Nazir, M. Salman, M. Athar, U. Farooq, A. Wahab, M. Akram, *Water Air Soil Pollut.* **2019**, *230*, 303. **DOI:**10.1007/s11270-019-4360-1
53. E. C. Lima, B. Royer, J. C. Vaghetti, N. M. Simon, B. M. da Cunha, F. A. Pavan, *J. Hazard. Mater.* **2008**, *155*(3), 536–550. **DOI:**10.1016/j.jhazmat.2007.11.101
54. B. H. Hameed, A. A. Ahmad, *J. Hazard. Mater.* **2009**, *164*(2-3), 870–875. **DOI:**10.1016/j.jhazmat.2008.08.084
55. M. M. Abd El- Latif, A. M. Ibrahim, *Desalin. Water Treat.* **2012**, *6*(1-3), 252–268. **DOI:**10.5004/dwt.2009.501
56. D. Pathania, S. Sharma, P. Singh, *Arab. J. Chem.* **2017**, *10*(1), S1445–S1451. **DOI:**10.1016/j.arabjc.2013.04.021
57. V. Vilar, C. Botelho, R. Boaventura, *J. Hazard. Mater.* **2007**, *147*(1-2), 120–132. **DOI:**10.1016/j.jhazmat.2006.12.055
58. G. B. Kankılıç, A. Ü. Metin, İ. Tüzün, *Ecol. Eng.* **2016**, *86*, 85–94. **DOI:**10.1016/j.ecoleng.2015.10.024
59. M. Al-Ghouti, M. A. Khraisheh, M. N. Ahmad, S. Allen, *J. Colloid Interface Sci.* **2005**, *287*(1), 6–13. **DOI:**10.1016/j.jcis.2005.02.002
60. Y. Bulut, H. Aydın, *Desalination* **2006**, *194*(1-3), 259-267. **DOI:**10.1016/j.desal.2005.10.032
61. T. Maneerung, J. Liew, Y. Dai, S. Kawi, C. Chong, C. H. Wang, *Bioresour. Technol.* **2016**, *200*, 350–359. **DOI:**10.1016/j.biortech.2015.10.047
62. X. Liu, C. He, X. Yu, Y. Bai, L. Ye, B. Wang, L. Zhang, *Powder Technol.* **2018**, *326*, 181–189. **DOI:**10.1016/j.powtec.2017.12.034
63. J. Mattson, H. Mark, Marcel Dekker, Ins., New York. **1971**.
64. J. Gong, J. Liu, Z. Jiang, X. Wen, E. Mijowska, T. Tang, X. Chen, *J. Colloid Interface Sci.* **2015**, *445*, 195–204. **DOI:**10.1016/j.jcis.2014.12.078
65. M. Danish, T. Ahmad, S. Majeed, M. Ahmad, L. Ziyang, Z. Pin, S. S. M. Iqubal, *Bioresour. Technol. Rep*. **2018**, *3*, 127–137. **DOI:**10.1016/j.biteb.2018.07.007
66. T. Benhalima, H. Ferfera-Harrar, *Int. J. Biol. Macromol.* **2019**, *132*, 126–141. **DOI:**10.1016/j.ijbiomac.2019.03.164
67. S. Lapwanit, T. Sooksimuang, T. Trakulsujaritchok, *J. Environ. Chem. Eng.* **2018**, *6*(5), 6221–6230. **DOI:**10.1016/j.jece.2018.09.050

Povzetek

V raziskavi je bila biomasa iz vrste *Phragmites australis* kemično modificirana z NaOH in za tem še s citronsko kislino, da bi proizvedli učinkovit adsorbent, imenovan SA-RPB. Absorbent je bil karakteriziran z metodami XRD, SEM, BET in FT-IR. Dokazano je bilo, da adsorbent obstaja predvsem v obliki kristalov celuloze, vsebuje mikropore s povprečnim premerom 15,97 nm in ima veliko število hidroksilnih in karboksilnih skupin na površini. Adsorpcijski proces SA-RPB smo ovrednotili z adsorpcijo barvila metilen modrega (MB) v vodni raztopini. Kinetika adsorpcije je bila opisana z modelom psevdo-drugega reda. Adsorpcijska izoterma je skladna z Langmuirjevim modelom z največjo adsorpcijsko zmogljivostjo 191,49 mg/g pri 303 K. Ugotovitve kažejo, da je MB mogoče učinkovito odstraniti iz vodnih raztopin z uporabo adsorbenta, izdelanega iz surove biomase *Phragmites australis*, obdelane z NaOH in nato s citronsko kislino.